Science Bulletin 65 (2020) 367–372

Contents lists available at ScienceDirect

Science Bulletin

journal homepage: www.elsevier.com/locate/scib

Science Bulletin
www.scibull.com

Article

Discovery of space aromaticity in transition–metal monoxide crystal Nb_3O_3 enabled by octahedral Nb_6 structural units

Zongxiang Hu, Guoyu Qian, Shunning Li, Luyi Yang, Xin Chen, Mouyi Weng, Wenchang Tan, Feng Pan *

School of Advanced Materials, Peking University, Shenzhen Graduate School, Shenzhen 518055, China

ARTICLE INFO

Article history:
Received 3 August 2019
Received in revised form 27 September 2019
Accepted 21 October 2019
Available online 2 November 2019

Keywords:
Nb–Nb metallic bonding
Octahedral Nb_6
Transition–metal monoxides
Aromaticity
Structural unit

ABSTRACT

An octahedral Nb_6 structural unit with space aromaticity is identified for the first time in a transition–metal monoxide crystal Nb_3O_3 by *ab initio* calculations. The strong Nb–Nb metallic bonding facilitates the formation of stable octahedral Nb_6 structural units and the release of delocalization energy. Moreover, the Nb atoms in continuously connected Nb_6 structural units share their electrons with each other in a continuous space of framework, so that the electrons are uniformly distributed. The newly discovered aromaticity in the octahedral Nb_6 structural units extends the range of aromatic compounds and broadens our vision in structural chemistry.

1. Introduction

The concept of aromaticity is continuously developing and changing. Aromaticity was initially introduced from benzene by Faraday in 1825 [1], and the term "Aromaticity" comes from the aromatic smells of benzene and its derivatives. Aromaticity subsequently refers to unusual chemical and structural inertness related to planar cyclic benzene molecule, which was first conceived by Kekulé in 1865 [2]. For the next 70 years, the physical origin of aromaticity had not been revealed, yet until Hückel [3] proposed delocalized conjugated bonding. Huker's rule is a semi–empirical rule of organic chemistry and its physical essence bases on a hypothesis that several orbitals interact with each other and share their electrons in a closed system [4]. For simple systems, quantum mechanics can treat these orbitals using linear combination and finally give the newly generated delocalized orbitals by performing variational method, but it cannot treat complicated systems directly due to massive demands on calculation. The semi-empirical Hückel's rule claims that the benzene, its derivatives, and other planar aromatic compounds should conform to the $(4n + 2)$ rule for electron counting [4]. However, accompanied by the discovery of aromaticity in high–dimensional molecules around the millennium, the Hückel's rule and the range of aromatic compounds have been developed simultaneously. For three-dimensional (3D) icosahedral fullerene, spherical aromaticity follows a $2(n + 1)^2$ rule for all conjugated π–electrons [5]. In 2005, the aromatic concept then has been expanded from organic molecules to metal-doped organic compounds. Möbius aromaticity describes that the conjugated organic molecule doped with the transition–metal *d* orbital twists all planar cyclic orbitals to stabilize its structure, and a $4n$ rule for electron counting is more favorable than $(4n + 2)$ rule for this system [6].

Actually, aromaticity exists in not only single-molecules but also in submicroscopic clusters. In 1987, quasi–aromatic $Mo_3S_4^{4+}$ clusters which showed benzene–like reactivity, structure, and stability were firstly proposed by Chen and Jiang et al. [7–9]. In recent years, the concept of aromaticity has been extended to all–metal cluster $[MAl_4]^{2-}$ (M = Cu, Li, Na) and led to further discoveries of all-metal aromaticity, such as XAl^{3-} (X = Si, Ge, Sn, Pb), metallophene (Rh_7, Pt_7, Pd_7), and aurophene (Au_x) [10–13]. Besides the main group metals, the $4d/5d$ transition–metals can also give rise to the *d*–orbital planar aromaticity, such as $[M_3O_9]^-$, $[M_3O_9]^{2-}$ (M = W, Mo) and X_4Li_2 (X = Cu, Ag, Au) [14,15]. Moreover, 3D aromaticity was reported in the cubic $[Zn_8^{II}(HL)_4(L)_8]^{12-}$ (L = tetrazole dianion) cluster and the tetrahedral cluster Au_{20} [16,17].

Transition–metal monoxide (TMMO) crystals tend to contain random vacancies in their rocksalt structure that possesses octahedrally coordinated TM atoms, which are always considered stoichiometrically instable and electrically insulating. For instance, the melting point of some TMMO crystals are: VO ~ 1223 K, FeO ~ 1642 K, CuO ~ 1500 K, respectively [18,19]. However,

* Corresponding author.
E-mail address: panfeng@pkusz.edu.cn (F. Pan).

https://doi.org/10.1016/j.scib.2019.10.026
2095-9273/

niobium monoxide Nb_3O_3 crystal is an exception, which shows a vacancy–ordered rocksalt prototypical structure and adopts octahedral Nb_6 structural units (shown in Fig. 1) and square–planar coordinated Nb atoms (NbO_4) to achieve anomalous thermostability with a melting point of 2213 K (significantly higher than TMMO crystals mentioned above). It also shows an anomalously stable phase structure: it can survive a high pressure up to 7.7 GPa without a phase transition. In particular, the Nb_3O_3 crystal keeps remarkable metallic property down to 1.38 K, below which it becomes a superconductor [20]. Researchers have never stopped trying to explain these anomalous properties of Nb_3O_3 during the past decades [21–23]. For instance, Schulz and Wentzcovitch [22] proposed a vacancy band theory to explain the conductive mechanism. However, most of the previous studies overlooked the electronic structural details entangled with the structural features. On the other hand, we recognized that the Nb_3O_3 crystal shows unusual chemical and structural inertness like benzene, and provided a new explanation to clarify the internal mechanism of thermal stability, phase stability and electric conductivity of Nb_3O_3 crystal via the scope of aromaticity.

2. Materials and methods

An aromatic compound shows the following three specific characteristics: (i) enhanced chemical stability compared to similar non–aromatic compounds; (ii) released delocalization energy from similarly structured compounds; (iii) a sufficiently delocalized electronic system [24–27]. To verify the presence of aromaticity in Nb_3O_3 crystal, we investigated the electronic structure of the square–tetra coordinated Nb atoms with four O ions (NbO_4) and an octahedral Nb_6 structural unit of Nb_3O_3 using *ab initio* calculations. It is identified that strong Nb–Nb metallic bonding exists in Nb_3O_3 crystal and it facilitates the formation of octahedral Nb_6 structural units with aromaticity. The presence of more delocalized Nb–Nb bonding can release delocalization energy from Nb_6 structural unit compared with similar structure that shares the prototypical structure with Nb_3O_3. The electronic states of Nb_6 structural unit are further analyzed by visualizing its real-space wave functions, which shows that the electrons are delocalized in the Nb_6 structural unit and contribute to conductive property. The delocalized electron system of an octahedral Nb_6 structural unit can be approximately considered as an electron gas, which surrounds the 3D Nb_6 structural unit. As a result, we call the aromaticity of the Nb_6 structural unit as space aromaticity.

Self-consistent generalized gradient approximation (GGA) approximations are applied in the first principle calculations, with the projector augmented wave approach [28–30]. For the exchange-correlation (XC) potential, we chose the Perdew–Burke–Ernzerhof function of the generalized-gradient approximations for ionic position optimization and electronic structure calculation [31]. The total energy for the investigated systems was converged to less than 10^{-5} eV with a plane-wave energy cutoff of 520 eV. A convergence threshold of 0.02 eV $Å^{-1}$ in force was reached for structure relaxation. In all calculations, a $6 \times 6 \times 6$ k-point mesh within the Monkhorst-Pack scheme is used for structure relaxation, and k-point sampling $8 \times 8 \times 8$ in the irreducible Brillouin zone (BZ) is applied to obtain a self-consistent charge density [32].

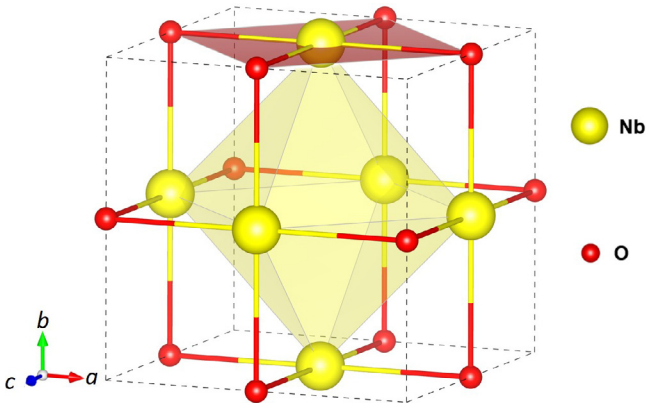

Fig. 1. The conventional rock salt unit cell for the niobium monoxide Nb_6 octahedral coordination with NbO_4 square-planar coordination.

3. Results and discussion

The remarkable stability of Nb_3O_3 demonstrates that strong bonding exits in Nb_3O_3. Inspired by chemical bond theory, the formation of bonding between two ions needs to fulfill two criteria: (i) energy match and (ii) spatial superposition (symmetry match) between orbitals involved in bonding.

To uncover the origin of the stability of Nb_3O_3, it is necessary to understand different environments of coordinated Nb with O ions, so the usual octahedral coordinated Nb with O ions was introduced to serve as a reference. The octahedrally coordinated NbO_6 structure shares a prototypical structure with Nb_3O_3 (shown in the Supplementary materials), which can determine whether square–planar NbO_4 structure in Nb_3O_3 releases delocalization energy from its prototype structure through more delocalized bonding. In this work, for clarity, square–planar Nb atoms and its counterpart octahedral Nb atoms are referred to as square–coord unit and octa–coord unit (NbO_6) as shown in Fig. 2a, respectively, to understand how the different coordination environment affects the electron configuration of the Nb ion. The schematic energy–level diagram of coordination transition is depicted in Fig. 2a. The NbO_6 possesses high point group symmetry O_h and it splits five

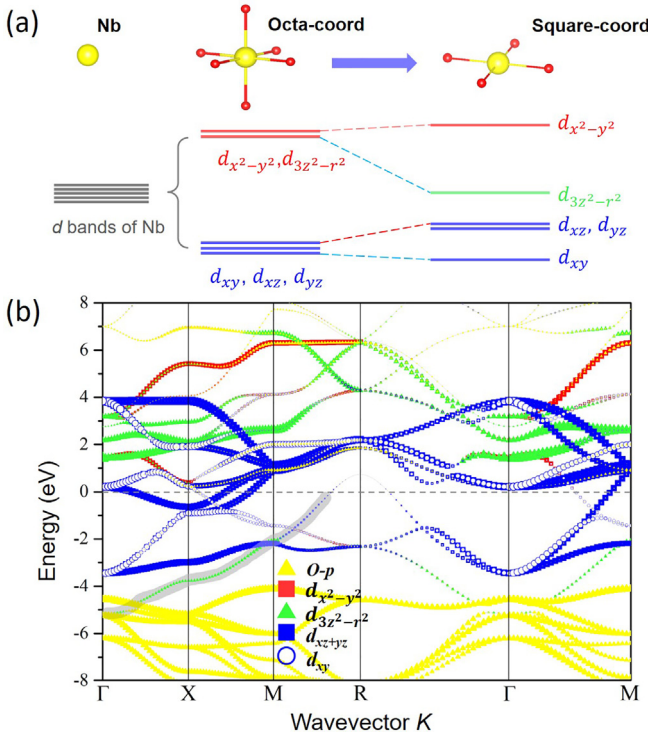

Fig. 2. The coordinated Nb energy levels and corresponding band structure. (a) The energy level schematic diagram depicts the coordination transition from octahedron to the planar square. (b) Calculated orbital–character–distinguished band structure of Nb_3O_3. The gray shadow highlights the low–laying $d_{3z^2-r^2}$ band.

d orbitals into two groups: the higher energy group e_g and the lower energy group t_{2g}. The doublet e_g state is composed of $d_{3z^2-r^2}$ and $d_{x^2-y^2}$ orbitals. The feature of this doublet state is that orientations of the two orbitals are spread out to ligands. The $d_{3z^2-r^2}$ points to ligands along z-axis and $d_{x^2-y^2}$ orients to ligands distributed in xy plane directly. The t_{2g} state is the opposite to e_g, and all orbitals in t_{2g} do not point to ligands directly. Shorter distances between e_g orbitals and ligand upraise their interaction energy with ligands, making their energy higher than t_{2g}. In NbO_4, the ligands along z axis are removed from the octahedron and then a planar square forms. Since $d_{3z^2-r^2}$ orbital is directly affected by the removal of ligands along z axis, its energy moves down. Meanwhile, d_{xz} and d_{yz} orbitals are separated from the original t_{2g} state. As the schematic energy–level diagram describes, separated $d_{3z^2-r^2}$ in square–coord can match the group (d_{xz}, d_{yz}) more easily in energy, while this match does not exist in octa–coord due to a large gap between e_g and t_{2g} orbitals.

Fig. 2b shows the calculated orbital–character–distinguished band structure of Nb_3O_3 crystal. The calculated band structure is in good agreement with previous works [22,23]. The Fermi energy (E_f) passes through both d bands, leading to metallic states. A large proportion of O–p is occupied and low lying. It should be noted that the Nb–d bands mostly depart from the O bands and show "ionic" gap [24]. This indicates that the Nb–O bonding is ionic. Occupied t_{2g}–p hybridized bands are above E_f and bonding states between Nb and O completely disappear in the vicinity of E_f. Because electronic states approaching E_f determine the conductivity of the solid, in this case the conductivity would be controlled by the Nb states only. Interestingly, a very dispersive band composed of $d_{3z^2-r^2}$ and d_{xz+yz} orbitals between energy range –6 eV and E_f can be observed. It testifies that separated $d_{3z^2-r^2}$ matches the energy and forms bonding with the group (d_{xz}, d_{yz}) in Nb_3O_3, in accordance with the former analysis of coordination. This band is highlighted with a grey shadow. The low–lying $d_{3z^2-r^2}$ orbitals hybridize with d_{xz+yz} between different Nb ions. The large bandwidth indicates that the d–d interactions are quite strong in Nb_3O_3. For comparison, the calculated band structure of octa–coord does not have this band, as seen in the Supplementary materials.

To further probe the intensity of Nb–Nb bonds, crystal orbital Hamilton population (COHP) calculations based on the framework of Perdew–Burke–Ernzerhof (PBE) were performed [33–36]. Positive values represent the bonding states and negative values show the antibonding interaction. In Fig. 3a, the broad bonding regime (–5 eV to Fermi level) corresponds to the delocalized interaction between Nb ions. Above the Fermi energy, negative COHP indicates the repulsion antibonding states of Nb–Nb interactions. Fig. 3b shows the detailed orbital comparison between $d_{3z^2-r^2}$-d_{yz} and $d_{3z^2-r^2}$–d_{xy} interactions. The $d_{3z^2-r^2}$-d_{yz} interaction is obviously stronger than $d_{3z^2-r^2}$-d_{xy} interaction. Fig. 3c and b show $d_{3z^2-r^2}$-d_{xy} and $d_{3z^2-r^2}$-d_{yz} interactions refer d_{xz}–p_z to Nb–O bonding, and indicate significant intensity of the $d_{3z^2-r^2}$-d_{yz} interaction. The results of COHP indicate that Nb_3O_3 can obtain "extra" stoichiometric stability from evidently stronger Nb–Nb bonding. The formation of strong Nb–Nb bonds can effectively release the energy of the square–coord system, which is 1.61 eV lower than the octa–coord (seen in the Supplementary materials), due to low–lying $d_{3z^2-r^2}$ bonding, contributing to high stoichiometric stability of Nb_3O_3.

The band structure demonstrates that NbO_4 square–planar coordination reduces the energy of $d_{3z^2-r^2}$ to match orbitals separated from t_{2g} states. How does space symmetry match criteria contribute to the formation of strong Nb–Nb bonding? Fig. 4a displays symmetry match of d–d interaction configurations in the cage-like Nb_6 octahedron. The type $d_{3z^2-r^2}$-d_{xz} interactions are effective, in which the lower (upper) $d_{3z^2-r^2}$ orbital can match all four middle planar d_{xz} orbitals. So in the Nb_3O_3, due to the existence of low energy $d_{3z^2-r^2}$ orbital, Nb–Nb metallic bonds can be significantly strengthened through efficient $d_{3z^2-r^2}$-d_{xz} overlap, whereas this match does not exist in octa–coord because of the large gap between e_g and t_{2g}. To further study the details of the orbital space distribution, the straightforward ELF was used [37]. Fig. 4b shows a plot of the ELF section along the (1 0 0) direction crossing four Nb and one O vacancy in the unit cell of Nb_3O_3. Interestingly, ELF

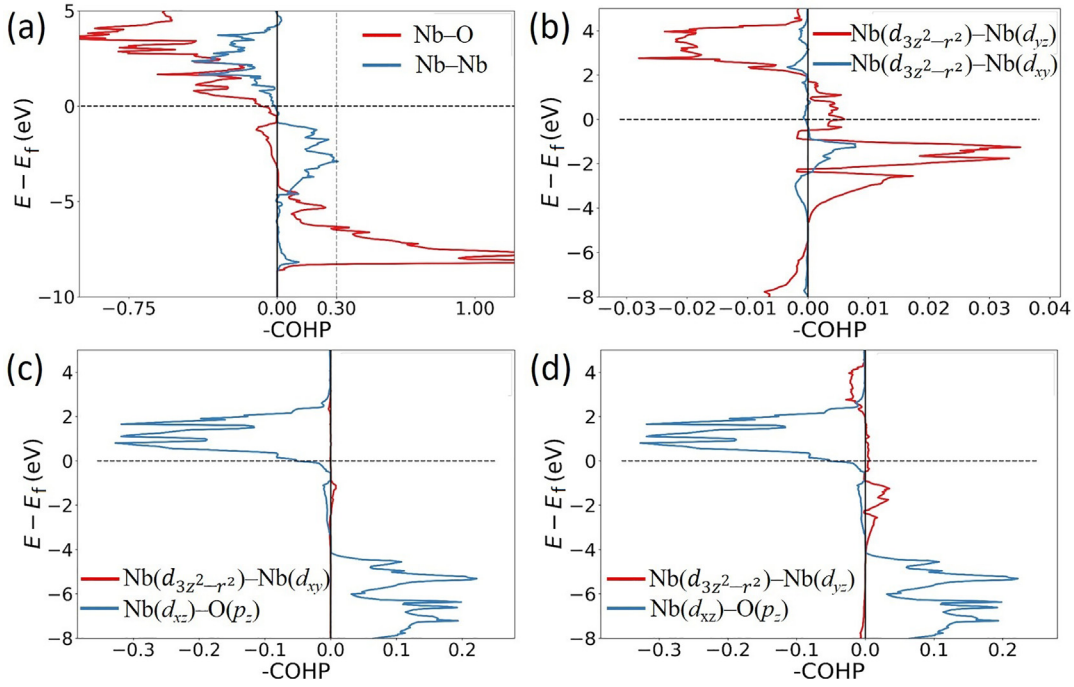

Fig. 3. COHP analyses of the Nb–Nb/Nb–O pairs of Nb_3O_3 with NbO_4 square-planar coordination. (a) The sum of all orbitals contributions for Nb–Nb, and Nb–O bonding. (b) The comparison between $d_{3z^2-r^2}$-d_{yz} and $d_{3z^2-r^2}$-d_{xy} interactions. (c) The interaction of $d_{3z^2-r^2}$-d_{xy} refers to d_{xz}–p_z of Nb–O bonding. (d) The interaction of $d_{3z^2-r^2}$-d_{yz} refers to d_{xz}–p_z of Nb–O bonding. The positive value represents the bonding state and the negative value shows the antibonding state.

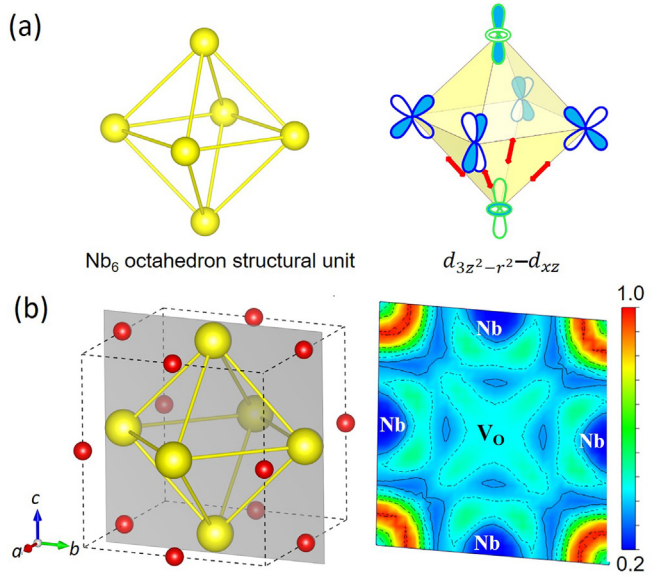

Fig. 4. The Nb_6 octahedron and *d*–*d* interaction. (a) The *d*–*d* interaction configuration in the cage-like Nb_6 octahedron. (b) The section along (1 0 0) direction crossing four Nb and one O vacancy in the unit cell of Nb_3O_3 and the 2D display of electronic localization function (ELF) along the section shown in the unit cell.

demonstrates the existence of direct Nb–Nb bonding and it is very similar to the ELF of Zn–Zn bonding in the aromatic $[Zn_8]^{8+}$ cluster [16]. The ELF shows a significantly dispersive distribution of Nb–*d* electrons through the entire O vacancy in the frame of Nb_3O_3. The Nb–O interaction shows typical characteristic of ionic bonding, which is consistent with ionic Nb–O bonding revealed by band structure analysis. It is worth noticing that the electrons of the Nb ions are quite delocalized and tend to interact with each other directly in a niobium monoxide system. Upon the removal of oxygen from the rock salt framework, the normally confined Nb–*d* electrons can further outspread over the space formerly occupied by oxygen ions. The ELF plot clearly displays Nb–Nb delocalization interaction, which explicitly manifests Nb–Nb interactions relying on O vacancies as a space medium. As shown in Fig. 4b, in fact, six Nb ions compose an Nb–octahedron in the unit cell with NbO_4 square–coord, forming the inner interacted Nb_6 metal structural unit. The other typical interactions can be found in the Supplementary materials and their differences are compared.

One would ask why other TMMOs, like VO, NiO, MnO do not form similar ordered–vacancies in their rock salt structure, then the TM_6 structural unit? Here, it is very important to point out that the *d* orbitals of Nb ions are more delocalized than other transition metals. The usual TMMOs, like NiO, are Mott insulators due to their localized *d* orbitals [21]. In these TMMOs, TM ions cannot interact with each other directly and TM–O covalent bonding is stronger due to intensive hybridization between local TM–*d* and O–*p* orbitals. The covalent electrons are such localized between TM and O ions that these electrons cannot overcome Coulombic repulsion from the covalent electrons of another site, leading to Mott insulator state. Thus, these TMMOs cannot enhance TM–TM bonding by the removal of oxygen. Moreover, the removal of oxygen weakens the covalent bonding between TM–O and decreases their thermal stability. Unlike these typical TMMOs, the Nb and O ions do not intensely hybridize with each other and more ions bonding correlates them in Nb_3O_3, resulting in that the Nb_6 cluster is comparatively isolated from the O framework and the migration of electrons only relies on Nb–Nb direct bonding. Therefore, the metallic state of Nb_3O_3 crystal is determined by Nb_6 structural units without considering the oxygen ions.

Although it is crucial for understanding the properties of the solids, the structural units of them are usually inaccessible. In our previous work, we have applied machine learning to get the relationship between atomic and electronic structures and uncover unusual structural units from exceptions [38]. Our previous work on cathode material $LiNi_{0.5}Mn_{0.5}O_2$ has revealed that the *d*–*p*–*d* Möbius aromaticity within the fragmented Mn_6–ring units contribute to stability and the interlayer ordering of the material [39]. In this work, by combining the ELF with the band theory, we can build the bonding motif of Nb_3O_3 crystal, in which fragmented Nb_6 structural units associated with properties are locally arranged inside the frame of oxygen, but electrons can be delocalized within its interior. This result is interesting because crystal materials or periodic solids, traditionally, are deemed as completely delocalized and indivisible entities. Our results suggest that, actually, they could be localized and divided into a hierarchical system of structural units. Therefore, a special structural unit in the solid can be selected to accurately represent the properties of solid in a much simpler way. Other works also demonstrated the aromatic structural units can exist in 2D materials and stabilize their structures. For example, local triple aromaticity enables planar tetra–coordinated metal carbide or metal nitrides like Co_2C or Co_2N, and periodic analog of π–aromaticity also exists in 2D surface Co_2C, Ni_2C, Co_2B, and Ni_2B [40,41]. Because Nb_6 structural unit

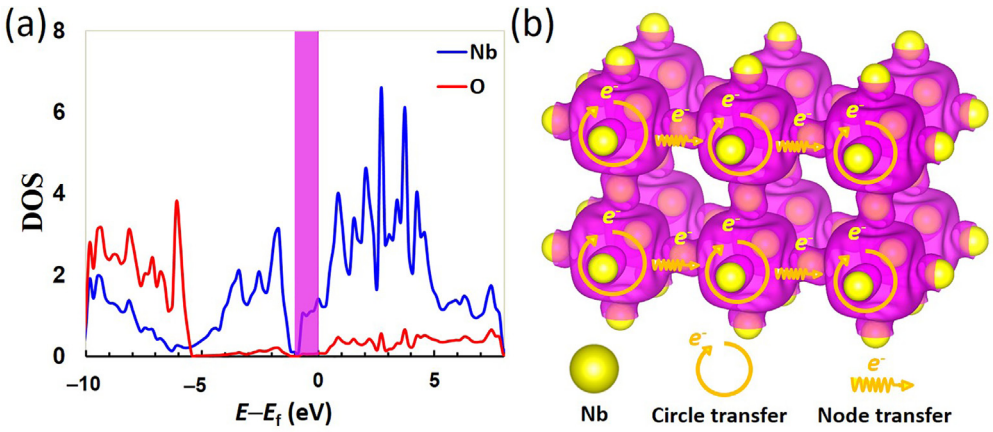

Fig. 5. The calculated densities of states and the partial charge density. (a) The projected densities of states (PDOS) calculated for square–coord. The purple shadow highlights the occupied states in the vicinity of the Fermi level. (b) The partial charge density (PCD) highlighted in the purple shadow. The Nb_6 structural unit includes the electronic states in the chamber and Nb_6 vertexes. The Nb_6 structural units connect each other with Nb nodes. Yellow circles represent electron transfer inner Nb_6 structural units and arrows represent electron transfer between Nb_6 structural units. The chamber electrons transfer throughout the Nb_6 network by virtue of Nb nodes.

contributes to the high stability of Nb_3O_3 crystal, it simultaneously possesses high symmetry and comparatively closed cyclic structure, which are features in accordance with properties defined by aromaticity. So, to clearly understand Nb_6 structural unit, it is needed to analyze its delocalized wave function, through which one can visually examine the interaction of the structural unit [42]. Fig. 5a shows the PDOS of Nb_3O_3 crystal and PCD of occupied states approaching the E_f. The calculated feature of PDOS is consistent with a former band structure of Nb_3O_3 crystal. We can see that the O–*p* states densely concentrate below –5 eV. The majority of Nb–*d* states distributed below –2 eV overlapping with O–*p* states. From –2 to –6 eV, we can find slight superposition between Nb and O, which is due to the inner Nb_6 interaction as analyzed above by band theory. The isolated states emerge at about –1 eV below E_f, in which there are dominantly Nb–*d* states and no O–*p* states. Since properties of the solid depend on these electronic states near E_f, it is necessary to visualize the real-space wave functions in order to understand the bonding distributions within the solid. The PCD is a straightforward way to visualize the selected wave function. As shown in Fig. 5b, the visualized isolated Nb_6–*d* wave function explicitly demonstrates that the six Nb atoms share their electrons with each other and Nb_6 structural unit also delocalizes its electrons into its chamber. The delocalized electronic behavior of Nb structural unit satisfies the intrinsic property of aromaticity. Clearly, these active electrons near E_f do not connect to the oxygen ions, so they can be seen as "local" within the Nb_6 structural unit. As a result, the Nb_6 structural unit is an integral composed of Nb–Nb bonding electrons and central chamber electrons. In addition, Nb_6 structural units share one Nb node to connect with each other and constitute an Nb_6 network so chamber electrons can transfer throughout aromatic Nb_6 structural unit network by Nb nodes (Fig. 5b). Therefore, both chamber electrons and electrons retained by Nb nodes contribute to the formation of Nb_6 network in whole Nb_3O_3 crystal and further lead to the metallic state of the solid.

4. Conclusions

To summarize, we have established an octahedral Nb_6 structural unit model with NbO_4 square–planar coordination in niobium monoxide Nb_3O_3, which provides a structural perspective to describe the band features more simply and accurately. We built the bonding motif of Nb_3O_3, in which Nb_6 structural unit is not only sufficiently isolated from the oxygen frame, but also able to be delocalized within its interior structure. The Nb_6 structural unit shows a highly symmetric structural features and releases delocalization energy through delocalized electronic states, indicating the aromatic property. Moreover, the electrons can be transferred between aromatic structural units via Nb atoms at the vertex of the Nb_6 structural units, which reveals the conductive mechanism of Nb_3O_3. Hence, we could make a proposal that the aromatic Nb_6 structural unit and its connection network might lead to that the Nb_3O_3 crystal become superconductive at 1.38 K. More importantly, the aromatic Nb_6 structural unit in Nb_3O_3 is distinct from the other members in the family of crystal structures, which would have its own unique usage in new material design and structural evolution.

Conflict of interest

The authors declare that they have no conflict of interest.

Acknowledgments

This work was financially supported by National Key R&D Program of China (2016YFB0700600), Soft Science Research Project of Guangdong Province (2017B030301013), and Shenzhen Science and Technology Research Grant (ZDSYS201707281026184).

Author contributions

Wenchang Tan and Feng Pan designed the research. Zongxiang Hu performed first-principles calculations and analyzed the results with the help from Shunning Li, Xin Chen, Guoyu Qian, Mouyi Weng and Luyi Yang. Zongxiang Hu wrote the manuscript. Wenchang Tan and Feng Pan revised the manuscript.

Appendix A. Supplementary materials

Supplementary materials to this article can be found online at https://doi.org/10.1016/j.scib.2019.10.026.

References

[1] Faraday M. On new compounds of carbon and hydrogen, and on certain other products obtained during the decomposition of oil by heat. Philos Trans R Soc 1825;115:440–66.
[2] Kekulé A. Sur la constitution des substances aromatiques. Bull Mens la Soc Chim Paris 1865;3:98.
[3] Hückel EZ. Quantentheoretische beiträge zum benzolproblem. Zeitschrift für Phys 1931;70:204–86.
[4] Coulson CA, O'Leary B, Mall RB. Hückel theory for organic chemists. Academic Press; 1978.
[5] Hirsch A, Chen ZF, Jiao HJ. Spherical aromaticity in I_h symmetrical fullerenes: the $2(N+1)^2$ rule. Angew Chem Int Ed 2000;39:3915–7.
[6] Rzepa HS. Möbius aromaticity and delocalization. Chem Rev 2005;105:3697–715.
[7] Chen ZD, Lu JX, Li J, et al. A comparative study of the aromaticity in some typical conjugated six–membered rings by the method of localized molecular orbital. Chin J Chem 1991;9:385–92.
[8] Chen ZD, Li J, Cheng WD, et al. A preliminary quantum chemical analysis of the nature of quasi–aromaticity of the puckered $[Mo_3S_3]$ ring in certain $[Mo_3S_4]^{4+}$ clusters. Chin Sci Bull 1990;35:1698–704.
[9] Jiang N, Schwarz WHE, Li J. Theoretical studies on hexanuclear oxometalates $[M_6L_{19}]^{q-}$ (M = Cr, Mo, W, Sg, Nd, U) electronic structures, oxidation states, aromaticity, and stability. Inorg Chem 2015;54:7171–80.
[10] Li X, Kuznetsov AE, Zhang HF, et al. Observation of all–metal aromatic molecules. Science 2001;291:859–61.
[11] Li X, Zhang HF, Wang LS, et al. Experimental and theoretical observations of aromaticity in heterocyclic XAl_3^- (X=Si, Ge, Sn, Pb) systems. Angew Chem Int Ed 2001;40:1867–70.
[12] Duan HH, Yan N, Yu R, et al. Ultrathin rhodium nanosheets. Nat Commun 2014;5:1–8.
[13] Zhai HJ, Kiran B, Dai B, et al. Unique CO chemisorption properties of gold hexamer: $Au_6(CO)_n^-$ (n = 0–3). J Am Chem Soc 2005;6:12098–106.
[14] Huang X, Zhai HJ, Kiran B, et al. Observation of *d*–orbital aromaticity. Angew Chem Int Ed 2005;44:7251–4.
[15] Wannere CS, Corminboeuf C, Wang ZX, et al. Evidence for d orbital aromaticity in square planar coinage metal clusters. J Am Chem Soc 2005;127:5701–5.
[16] Cui P, Hu HS, Zhao B, et al. A multicentre–bonded $[Zn^I]_8$ cluster with cubic aromaticity. Nat Commun 2015;6:6631.
[17] Li J, Li X, Zhai HJ, et al. Au_{20}: a tetrahedral cluster. Science 2003;299:864–8.
[18] Greenwood NN, Earnshaw A. Chemistry of the elements. Butterworth-Heinemann; 1997.
[19] Patnaik P. Handbook of inorganic chemicals. McGraw–Hill 2002.
[20] Hulm JK, Jones CK, Hein RA, et al. Superconductivity in the TiO and NbO systems. J Low Temp Phys 1972;7:29–307.
[21] Efimenko AK, Hollmann N, Hoefer K, et al. Electronic signature of the vacancy ordering in NbO (Nb_3O_3). Phys Rev B 2017;96:195112.
[22] Schulz WW, Wentzcovitch RM. Electronic band structure and bonding in Nb_3O_3. Phys Rev B 1993;48:16986–91.
[23] Wimmer E, Schwarz K, Podloucky R, et al. The effect of vacancies on the electronic structure of NbO. J Phys Chem Solids 1982;43:439–47.
[24] Krygowski TM, Cyrański MK. Structural aspects of aromaticity. Chem Rev 2001;101:1385–420.
[25] Schleyer PR. Introduction: aromaticity. Chem Rev 2001;101:1115–8.
[26] Chen ZF, Wannere CS, Corminboeuf C. Nucleus–independent chemical shifts (NICS) as an aromaticity criterion. Chem Rev 2005;105:3842–88.
[27] Boldyrev AI, Wang LS. All–metal aromaticity and antiaromaticity. Chem Rev 2005;105:3716–57.
[28] Blöchl PE. Projector augmented-wave method. Phys Rev B 1994;50:17953–79.
[29] Kresse G, Joubert D. From ultrasoft pseudopotentials to the projector augmented-wave method. Phys Rev B 1999;59:1758–75.
[30] Blöchl PE, Först CJ, Schimpl J. Projector augmented wave method: ab initio molecular dynamics with full wave functions. Bull Mater Sci 2003;26:33–41.

[31] Perdew JP, Burke K, Ernzerhof M. Generalized gradient approximation made simple. Phys Rev Lett 1997;78. 1396–1396.
[32] Monkhorst HJ, Pack JD. Special points for Brillouin-zone integrations. Phys Rev B 1976;13:5188–92.
[33] Dronskowski R, Bloechl PE. Crystal orbital Hamilton populations (COHP): energy–resolved visualization of chemical bonding in solids based on density–functional calculations. J Phys Chem 1993;97:8617–24.
[34] Deringer VL, Tchougréeff AL, Dronskowski R. Crystal orbital Hamilton population (COHP) analysis as projected from plane–wave basis sets. J Phys Chem A 2011;115:5461–6.
[35] Maintz S, Deringer VL, Tchougréeff AL, et al. Analytic projection from plane–wave and PAW wavefunctions and application to chemical–bonding analysis in solids. J Comput Chem 2013;34:2557–67.
[36] Maintz S, Deringer VL, Tchougréeff AL, et al. LOBSTER: a tool to extract chemical bonding from plane–wave based DFT. J Comput Chem 2016;37:1030–5.
[37] Becke AD, Edgecombe KE. A simple measure of electron localization in atomic and molecular systems. J Chem Phys 1990;92:5397–403.
[38] Jie JS, Hu ZX, Qian GY, et al. Discovering unusual structures from exception using big data and machine learning techniques. Sci Bull 2019;64:612–6.
[39] Hu ZX, Zheng JX, Xin C, et al. Inorganic aromaticity of Mn_6–ring cluster in layered $Li(Ni_{0.5}Mn_{0.5})O_2$. J Phys Chem C 2018;122:4125–32.
[40] Jimenez-Izal E, Saeys M, Alexandrova AN. Metallic and magnetic 2D materials containing planar tetracoordinated C and N. J Phys Chem C 2016;120:21685–90.
[41] Nandula A, Trinh QT, Saeys M, et al. Origin of extraordinary stability of square–planar carbon atoms in surface carbides of cobalt and nickel. Angew Chem Int Ed 2015;54:5312–6.
[42] Alexandrova AN. Divide–and–conquer chemical bonding models for materials: a tool for materials design at the electronic level. Chem Mater 2017;29:8555–65.

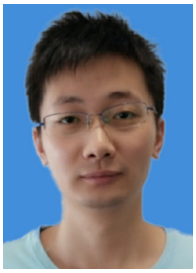

Zongxiang Hu received his B.S. degree in 2014 and is now pursuing his Ph.D. degree under the supervision of Prof. Feng Pan at School of Advanced Materials, Peking University Shenzhen Graduate School. His current researches mainly relate to the application of the first-principles calculation to investigate the thermodynamics and electrochemical properties of layered transition metal oxide cathode materials.

Feng Pan got his B.S. degree from Department of Chemistry, Peking University in1985 and Ph.D. degree from Department of P&A Chemistry, University of Strathclyde, UK, with "Patrick D. Ritchie Prize" for the best Ph.D. in 1994. Now he is a National 1000-plan Professor, Founding Dean of School of Advanced Materials, Peking University Shenzhen Graduate School, and Director of National Center of Electric Vehicle Power Battery and Materials for International Research. He is engaged in fundamental research and product development of novel energy conversion and storage materials & devices.